Polymer Chemistry

Accepted Manuscript

Volume 7 | Number 1 | 7 January 2016 | Pages 1–246

Polymer Chemistry

www.rsc.org/polymers

ISSN 1759-9954

ROYAL SOCIETY OF CHEMISTRY

PAPER
Munju Goh et al.
Enhancement of the crosslink density, glass transition temperature, and strength of epoxy resin by using functionalized graphene oxide co-curing agents

175 YEARS

ROYAL SOCIETY OF CHEMISTRY

rsc.li/polymers

Dispersible Microporous Di-block Co-Polymer Nanoparticles via Polymerisation-Induced Self-Assembly

Alex M. James,[1] Matthew J. Derry,[1] Jennifer S. Train[1] and Robert Dawson*[1]

Microporous materials are predominantly formed as insoluble powders which means that they can be difficult to process. Here we report a new class of solvent-dispersible porous polymers synthesised by reversible addition-fragmentation chain transfer mediated polymerisation-induced self-assembly (RAFT-mediated PISA), formed from a PEG macro-CTA polymerised with divinylbenzene and fumaronitrile. The particles have a dual morphology consisting of smaller spheres of 24-29 nm aggregated into larger particles of 204 - 262 nm. Gas sorption analysis showed the particles to have BET surface areas of 274 to 409 m2/g with internal pore sizes centred around 1.8 nm and further larger pores arising from the sphere packing of the aggregates. The particles were found to be photoluminescent (emission λmax = 326 nm) when exposed to UV light which could be quenched by the addition of nitroaromatic compounds. For example, 99% if the emission was quenched in the presence of 38 ppm of picric acid .

Introduction

The design and synthesis of microporous organic polymers (MOPs) is a growing area of research due to a combination of properties which include high surface area, chemical and thermal stability, low skeletal density and relative ease with which they can be functionalised, either by the judicious use of pre-functionalised monomers or via post-synthetic modification towards more complex functionalities.[1, 2] The combination of these properties has attracted considerable interest not only in fundamental research but also into the practical application of these materials in fields such as gas storage and separation,[3-8] chemosensing,[9-12] waste-water treatment[13, 14] and catalysis.[15, 16] Amongst MOPs many subclasses exist including hypercrosslinked polymers (HCPs)[17, 18] polymers of intrinsic microporosity (PIMs),[19, 20] conjugated microporous polymers (CMPs),[21-25] covalent organic frameworks (COFs)[26-31] and covalent triazine-based frameworks (CTFs).[32, 33] However, there are a number of disadvantages to some of these material sub-classes, such as the need for expensive monomers, metal catalysts, toxic solvents and lengthy polymerisation times which limits their use in many practical applications.

Another key disadvantage to most MOPs (with the notable exception of linear PIMs) is their complete insolubility in all solvents. This arises due to their highly crosslinked structure which is necessary to induce porosity in these materials. Linear PIMs avoid this problem by using a rigid and contorted monomer which allows soluble microporous polymers to be produced and cast into free standing films.[20] There are however only a few of these rigid contorted monomers available commercially limiting the range of soluble microporous

polymers which can be made. A number of other attempts have led to the fabrication of solution-processable microporous polymers including; the addition of solubilising side chains to monomers such as tetraphenyl-5,5-dioctylcyclopentadiene.[34] However, the long flexible chains that provide the solubility also fill the pores of the material resulting in a very low surface area. Cheng et al. used pyrene based monomers with solubilising t-butyl groups to produce a soluble CMP network using Suzuki coupling, however this route requires the use of expensive Pd catalysts and has a limited range of t-butyl monomers which can be used.[35] By using high dilution Yang et al. were able to hypercrosslink individual poly(styrene) chains which were found to be soluble in a range of solvents with surface areas up to around 700 m^2/g.[36] Though these porous polymers were found to lose their porosity over time. Mai *et al*. were able to synthesise microporous particles using a divergent 3-step procedure by firstly making vinylbenzyl chloride particles using emulsion polymerisation followed by hypercrosslinking with FeCl$_3$ in 1,2,dichloroethane.[37] Using the unreacted end groups it was possible to grow solubilising polymer chains via ATRP chemistry resulting in a core-shell structure with a surface area of 562 m^2/g. While this route demonstrated the concept of core-shell microporous particle dispersions, the use of the multi-step approach, harmful solvents and stoichiometric amounts of FeCl$_3$ is not ideal and due to the acidic conditions limits the possibility of functionalisation. The synthesis of soluble or dispersible microporous polymers is however, clearly still of great importance. Equally important is the need to develop a more generic method of synthesising MOPs which alleviates these issues and delivers a material which is able to be processed and applied in the solution form from simple building blocks in a one pot synthesis.

Recently, the group of Li and co-workers reported the synthesis of a series of microporous polymers from the widely available vinyl precursors divinylbenzene and fumaronitrile *via* conventional radical polymerisation thus avoiding some of the issues attributed to conventional HCP synthesis.[38] These polymers boast large surface areas as well as being cheap to synthesise. Furthermore, no by-products were formed from the reaction and there is no need for metal-catalysts or harmful solvents to be used in order to induce porosity. Yet, like most

a. Department of Chemistry, University of Sheffield, Sheffield UK. S3 7HF.
.

Polymer Chemistry Accepted Manuscript

porous materials, they are completely insoluble in common organic solvents, hence limiting their potential applications.

There have been a number of reports of porous polymer particles using diblock co-polymers based on polystyrene-poly(ethylene oxide) (PS-*b*-PEO) synthesized via atom-transfer radical polymerization (ATRP).[39, 40] In these cases, a hierarchically structured porous polymers is formed via the self-assembly of the diblock co-polymers in organic solvents followed by the hypercrosslinking of the PS. This leads to core-shell particles where the PS block forms a porous shell with the PEO forming the core of the particle.

We believe that the strategy of using block copolymers to synthesise porous polymers has much promise. By building on the reports of free radical porous polymers, outer solubilising chains, and diblock co-polymer self-assembly we aim to reverse the blocks and synthesise porous particles with a solubilising outer shell and a porous core. This can be achieved using a one step, metal-free radical addition fragmentation transfer-mediated polymerisation induced self-assembly (RAFT-mediated PISA) approach. Microporous polymers synthesised via this method have significant scope for future variation to produce a wide variety of functional dispersible microporous particles which could be used for a wide range of solution based applications as well as being solution processable.

Results and discussion

A RAFT-mediated PISA approach, without the need for metal catalysts and environmentally harmful carcinogenic solvents, [37] was carried out using a PEG based macro chain-transfer agent (macro-CTA), divinylbenzene (DVB) and fumaronitrile (FN) in a water/alcohol solvent mix. The PEG based macro-CTA was first synthesised using PEG monomethyl ether (average M_n = 5000) and 2-bromoisobutyryl bromide to form PEG-Br followed by a reaction with dodecanethiol and carbon disulphide (Figures S1-S3). The PEG macro-CTA, DVB and FN were dissolved in a 60:40 water:ethanol mix to create a 1 wt.% solution which was heated to 70 °C with 0.2 eq. of KPS as the water soluble initiator (Scheme 1c). After 24 h the resulting milky solutions were centrifuged and re-precipitated into ether to yield white solids in a 22-68 % yield. The solids were able to be redispersed into a range of solvents (including water, alcohols, THF, acetonitrile, halogenated solvents) and showed no visual change over a time of > 6 months thus demonstrating long term stability as homogeneous solutions.

In comparison, the conventional RAFT reaction in toluene which solubilises the PEG macro-CTA, FN and DVB results in a network structure where the PEG groups are randomly distributed throughout the network (Scheme 1b, conventional RAFT solution PEG$_{113}$DVB$_{300}$FN$_{225}$). This white solid precipitate does not form a stable dispersion over time (> 1 hour). Likewise, free radical polymerisation of FN and DVB in toluene, as reported previously by Li and co-workers,[38] yields an insoluble white powder (Scheme 1a, HCPN-0.75). It is therefore clear that not only is the macro-CTA required, but also a RAFT-mediated PISA approach is vital in order to form stable colloidal dispersions

The dispersibility of the RAFT-PISA series of samples was investigated by dispersing the samples in methanol (Scheme 1 insert). Stable homogenous solutions were formed after sonication of the methanol solution for 30 minutes and no visible settling of the particles was observed after one week (Figure S4). Conversely the sample containing no PEG (HCPN-0.75) and the sample synthesised via the conventional RAFT route both began to settle out immediately. This observation highlights the necessity of both the hydrophilic PEG chains as well as the RAFT PISA approach in order to form stable dispersions.

Table 1. Composition, solubility and size of particles.

Sample	Monomer composition			Dispersible[a]	Hydrodynamic diameter (D_h) (nm)[b]		SAXS Particle Size Analysis[c]			
	PEG	DVB	FN		After 30 min. sonication	After 3 hr sonication	D_1 (nm)	D_2 (nm)	D_{PY1} (nm)	D_{PY2} (nm)
HCPN-0.75[38]	0	1	0.75	No	N/A	N/A	N/A	N/A	N/A	N/A
PEG$_{113}$DVB$_{300}$FN$_{225}$ (RAFT solution)	113	24	18	<1 hr	N/A	N/A	N/A	N/A	N/A	N/A
PEG$_{113}$DVB$_{150}$FN$_{113}$	113	12	9	Yes	241	204	27	138	34	239
PEG$_{113}$DVB$_{300}$FN$_{225}$	113	24	18	Yes	229	219	29	174	34	242
PEG$_{113}$DVB$_{600}$FN$_{450}$	113	48	36	Yes	435	230	24	179	31	279
PEG$_{113}$DVB$_{1200}$FN$_{900}$	113	96	72	Yes	942	262	25	188	42	256

[a] dispersibility in water, [b] mean particle diameter as measured by DLS in methanol, [c] particle size as measured by SAXS where: D_1 is the mean diameter of the primary particles, D_2 is the mean diameter of the aggregates, D_{PY1} is the mean interaction distance between primary particles and D_{PY2} is the mean interaction distance between the aggregates
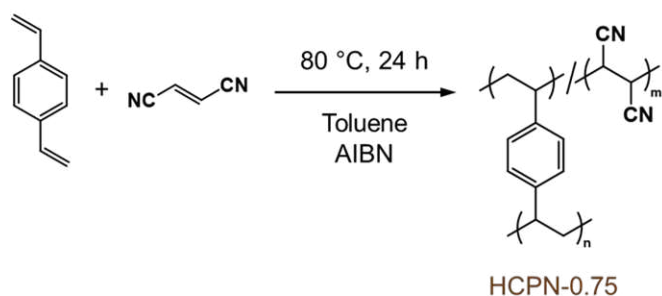
Scheme 1. Synthesis of porous materials via (a) free radical polymerisation to form insoluble HCPN-0.75,[38] (b) conventional RAFT solution chemistry and (c) RAFT mediated PISA. Insert shows the materials in methanol after 12 h.

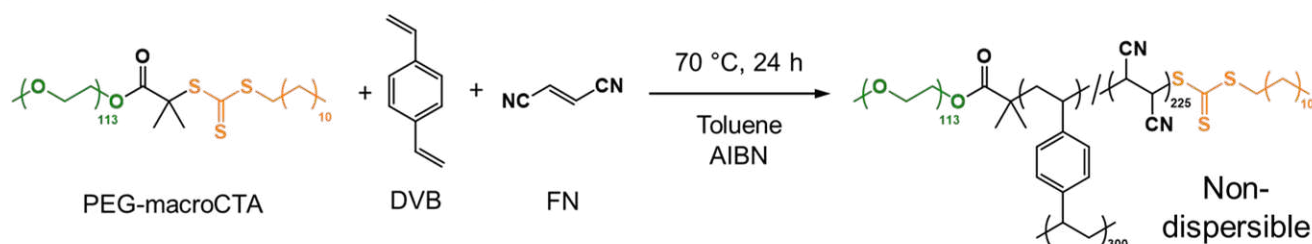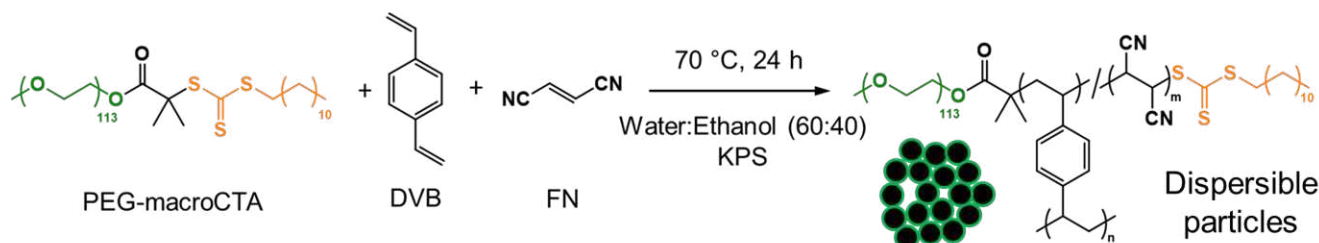To measure the size of the particles, dynamic light scattering (DLS) was carried out on the samples using 0.1 mg/mL solutions in methanol. Initially, all samples were sonicated for 30 minutes before analysis and the particle sizes were calculated to be between 241 nm for the smallest sample, $PEG_{113}DVB_{150}FN_{113}$ and 942 nm for the largest sample, $PEG_{113}DVB_{1200}FN_{900}$ (Table 1 & Figure S5). Such large particle sizes were not expected for samples containing DPs in the 300-2500 range. Further sonication was therefore carried out. After 3 hours of sonication the particle sizes had reduced to between 204-262 nm – still larger than expected for samples of similar DPs (Table 1 & Figure S6). Typical particle sizes for linear di-block polymer chains via RAFT-PISA in similar solvent mixtures give spherical particles with sizes of around 31 nm.[41] In addition, the particle sizes of hypercrosslinked PEO_{117}-b-PS_{395} synthesised by Gao et al.[40] observed particle sizes of around 24 nm, while for PEO-b-PS assemblies synthesised by Xu et al.[39] the core-shell sizes of the individual particles ranged from 29-37 nm for DPs of 478-834 but were aggregated together into a larger extended 3D network.

Although a reduction in size of the particles was observed after prolonged sonication, the overall sizes of the particles were still much larger than expected. Therefore, in order to further elucidate the particle morphology, SAXS studies on a 5% w/w dispersion of each sample in methanol were performed (Fig. 1a). To simplify the analysis, the particles were treated as homogeneous solid spheroids. The X-ray scattering intensity of such spheroids, represented by the scattering cross-section per unit sample volume, $\frac{d\Sigma}{d\Omega}(q)$, can be expressed as:

$$\frac{d\Sigma}{d\Omega}(q)_n = N_n S_{PY}(q)_n \int_0^\infty g_{Gauss}(R_n)|F(qR_n)|^2 dR_n \quad \text{(Eq. 1)}$$

where N_n is the number of scatterers, $S_{PY}(q)_n$ is the hard-sphere interaction structure factor based on the Percus-Yevick approximation,[42] $g_{Gauss}(R_n)$ is their Gaussian size distribution function and $F(qR_n)$ is the particle form factor. Specifically, $g_{Gauss}(R_n)$ is expressed as:

$$g_{Gauss}(R_n) = \frac{1}{\sigma_{R_n}\sqrt{2\pi}} e^{-\frac{(R_n - \bar{R}_n)^2}{2\sigma_{R_n}^2}} \quad \text{(Eq. 2)}$$
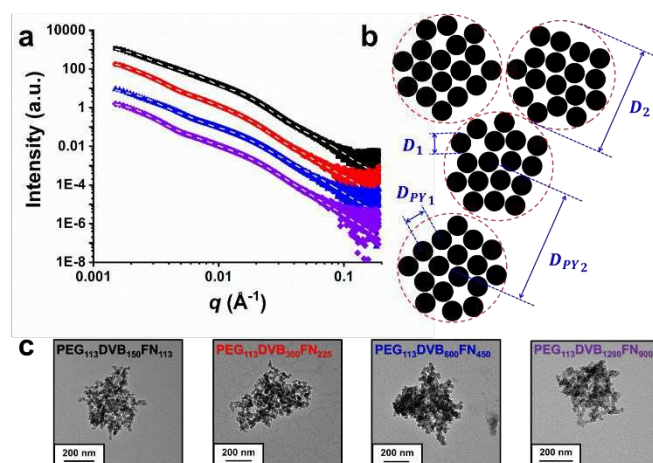
Figure 1. (a) Small angle X-ray Scattering of samples PEG$_{113}$DVB$_{150}$FN$_{113}$ (black), PEG$_{113}$DVB$_{300}$FN$_{225}$ (red), PEG$_{113}$DVB$_{600}$FN$_{450}$ (blue) and PEG$_{113}$DVB$_{1200}$FN$_{900}$ (purple), (b) schematic representation of particle morphology where: D_1 is the mean diameter of the primary particles, D_2 is the mean diameter of the aggregates, D_{PY1} is the mean interaction distance between primary particles and D_{PY2} is the mean interaction distance between the aggregates, (c) from left to right TEM images of PEG$_{113}$DVB$_{150}$FN$_{113}$, PEG$_{113}$DVB$_{300}$FN$_{225}$, PEG$_{113}$DVB$_{600}$FN$_{450}$ and PEG$_{113}$DVB$_{1200}$FN$_{900}$.

where $\overline{R}_n$ is the mean radius of the particles and σ_{R_n} is the standard deviation of the size distribution. The particle form factor, $F(qR_n)$, is expressed as:

$$F(qR_n) = \frac{4}{3}\pi R_n^3 \Delta\xi \left(3\frac{sin(qR_n) - qR_n cos\,(qR_n)}{(qR_n)^3}\right) \qquad \text{(Eq. 3)}$$

where $\Delta\xi$ is the X-ray scattering contrast.

Initial inspection of the background-subtracted SAXS pattern for a 5% w/w dispersion of each sample in methanol indicated that a complex morphology consisting of two populations was present: one of small particles (n=1 in Eq. 1-3) and the other of larger particles (n=2 in Eq. 1-3).

$$I(q) = \frac{d\Sigma}{d\Omega}(q)_1 + \frac{d\Sigma}{d\Omega}(q)_2 \qquad \text{(Eq. 4)}$$

This two-population approximation provided a satisfactory fit over the entire q-range and indicated that primary nanoparticles of between 24 nm and 29 nm in diameter (D_1) existed within larger aggregates whose diameter ranged from 138 nm to 188 nm (D_2) (see Figure 1b). The Percus-Yevick hard-sphere mean interaction distance between interacting primary particles (D_{PY1}) ranged between 31 nm and 42 nm, and that between larger aggregates (D_{PY2}) was found to be between 239 nm and 279 nm. TEM analysis was performed on the samples (Figure 1c), which confirmed that each sample consisted of aggregates of smaller assemblies as indicated by SAXS analysis.
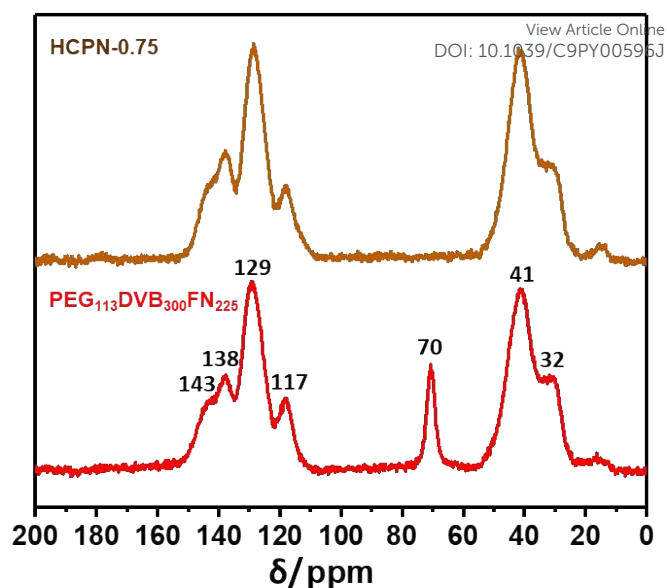

Figure 2. ^{13}C CP/MAS NMR spectra of insoluble HCPN-0.75 (top) and PEG$_{113}$DVB$_{300}$FN$_{225}$ (bottom)

The aggregated morphology found for the particles differs to those obtained by aqueous RAFT-PISA of similar but non-crosslinked systems such as styrene, which typically result in the formation of well-defined nanoassemblies.[41, 43] However, the post-synthetic hypercrosslinking of linear di-block PEO-b-PS polymers by Xu et al.[39] resulted in an aggregated morphology similar to that observed for our particles. We attribute our aggregated morphology to a high degree of crosslinking both within and between the particles arising from the bi-functional DVB monomer. The crosslinking of smaller spheres thereby creates an extended 3D network. Despite this unusual morphology, the particles are still able to form stable dispersions for long periods of time without precipitation due to the presence of the outer hydrophilic PEG block. This is in contrast to the PEO-b-PS particles of Xu and Gao which have core forming PEO blocks.[39, 40]

In order to probe the particle morphology in more detail, we synthesised di-block co-polymers targeting the same DP but substituting styrene for DVB. DLS analysis of these reactions showed the presence of particles of between 200 – 315 nm, similar to the DVB analogues. TEM analysis of these samples however, show spherical particles unlike the aggregated morphologies when using DVB (Figure S8 and Table S2).[41, 44] It is therefore likely that the polymerisation mechanism is different when using the bi-functional monomer DVB which causes the aggregated morphology rather than the typical spherical morphology seen in the literature for linear block co-polymers. To further probe the particle formation mechanism, the progression of the PEG$_{113}$DVB$_{1200}$FN$_{900}$ reaction over time was and the particle sizes calculated using DLS. After only 15 min, a particle size of around 80 nm was calculated, suggesting that crosslinking of particles occurs early in the reaction rather that the formation of spheres followed by subsequent aggregation. The particles continued to grow over the course of the reaction eventually reaching around 255 nm after 24 h.

The particle size behaviour in different solvents was also investigated. The particles were found to be dispersible in a variety of solvents including chloroform, dichloromethane, toluene, methanol, THF, acetonitrile and acetone. Stable dispersions were observed for methanol, THF, acetonitrile and acetone, while in chloroform, dichloromethane and toluene particle sedimentation was observed over a period of 24 h. In methanol, THF, acetonitrile and acetone, particle sizes of between 200-245 nm were calculated for $PEG_{113}DVB_{150}FN_{113}$ while in chloroform, dichloromethane and toluene the particle sizes were much larger ranging from 2111-2223 nm. In general, increasing the core DP increased the particle size in the stable solvents, however for chloroform, dichloromethane and toluene particle sizes varied widely. These solvents are likely to swell the core as reported for insoluble porous polymers.[4, 45-47] This swelling effect leads to the increase in calculated particle size and loss of long term stability in solution.

Chemical characterisation of the samples was carried out by elemental analysis, FTIR, and both solution and solid state NMR. The FTIR spectra of each sample (Figure S9) shows vibrational stretches at 2928 cm^{-1}, 2250 cm^{-1} and 1125 cm^{-1} attributed to the $-CH_2-$ stretch, $-C{\equiv}N-$ stretch and C-O ether stretch respectively demonstrating the successful incorporation of both fumaronitrile and macro-CTA. Elemental analysis (Table S4) of the samples also showed that the fumaronitrile monomer was incorporated into the structure with all samples containing nitrogen in amounts varying from 6.83% to 7.31%. Likewise, the RAFT agent had also been successfully incorporated into the final material and this was reflected by the sulfur content in the samples which varied from 0.26% to 0.79%.

Solution phase ^{1}H-NMR of the dispersions exhibited a resonance at 3.5 ppm which is assigned to the $-CH_2-$ of the PEG chains (Figure S10). In common with other microporous polymers the core of the particles is highly crosslinked and immobile and would not be expected to be observed by solution phase NMR. However, resonances at 0.9 and 1.3 ppm were observed and are attributed to the DVB/FN backbone, it is therefore likely that some mobility of the backbone is possible due to swelling of the sample in $CDCl_3$ as noted for the DLS results above (Table S3). To further investigate the core of the particles, solid state ^{13}C CP/MAS NMR was employed and compared to that of the insoluble HCPN-0.75 (Figure 2 and Figure S9). Both the insoluble network and the particles show resonances in the aromatic region for 143, 138, 129 and 117 ppm – these are attributed to the quaternary aromatic $-C_{Ar}-$, unreacted vinyl, aromatic $-C_{Ar-H}-$ and the nitrile groups respectively as previously reported.[38] The internal polymer backbone is also observed at 41 and 32 ppm. An additional resonance at 70 ppm is observed for $PEG_{113}DVB_{300}FN_{225}$ which we assign to the outer PEG $-CH_2-$ groups.

The porosity of each sample was investigated using gas sorption analysis using nitrogen gas at 77 K (Figure 3a). As expected for aggregated particles with a large number of inter-particle voids, there is a large uptake of gas adsorbed at high relative pressures (> 0.9 P/P_0) in all 4 samples resulting from the condensation of nitrogen between the particles similar to other aggregated particle networks.[39] In the low pressure region,

there is a sharp uptake of gas below 0.1 P/P_0 indicative of adsorption in the micropores.

Figure 3. (a) Nitrogen adsorption (filled) and desorption (open) isotherms at 77 K (each offset by 200 cm^3/g), insert shows the
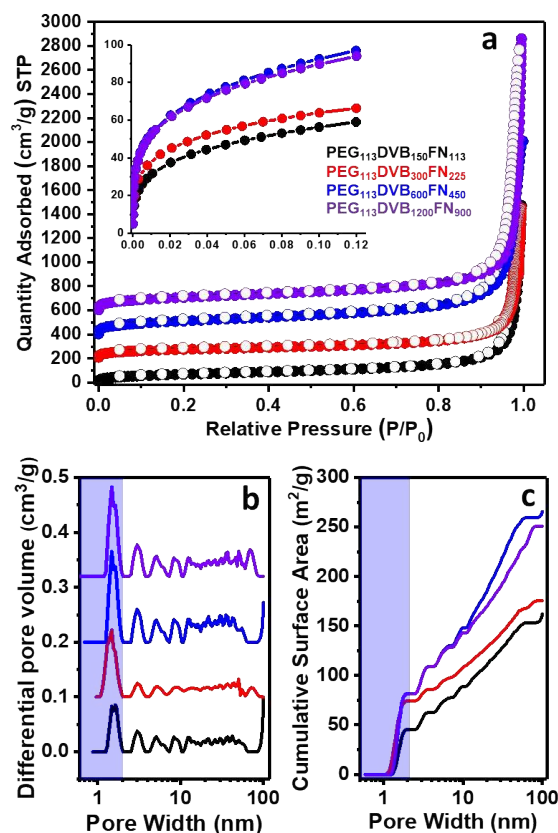
low relative pressure region, (b) NL-DFT differential pore size distribution and (c) cumulative surface area vs pore width for samples $PEG_{113}DVB_{150}FN_{113}$ (black), $PEG_{113}DVB_{300}FN_{225}$ (red), $PEG_{113}DVB_{600}FN_{450}$ (blue) and $PEG_{113}DVB_{1200}FN_{900}$ (purple).

The BET surface areas for all samples were calculated over a relative pressure range of 0.01 − 0.15 P/P_0 (see Table 2). The surface area of the smallest sample $PEG_{113}DVB_{150}FN_{113}$ was calculated to be 244 m^2/g. The particles show an increase in surface area with increasing core monomer content; up to around 400 m^2/g for the samples containing the largest amounts of core monomers - $PEG_{113}DVB_{600}FN_{450}$ allowing the tuning of the porosity by increasing the particle size. No further increase in porosity was observed for $PEG_{113}DVB_{1200}FN_{900}$ which could indicate that the maximum surface area has been achieved for this system. The increase in porosity is to be expected for larger particles which possess an increase in internal porosity arising from a larger porous core. In contrast, particles of increasing size possessing only external surface areas would be expected to show a decrease in surface area. The increase in surface area with respect to the DP of the porosity inducing block is similar to that observed for hypercrosslinked PEO-*b*-PS particles (DPs of 362-718 increasing surface areas from 50-132 m^2/g).[39] The BET surface areas of the

ARTICLE

particles compare well to other soluble microporous polymers in the literature (ca. 130-600 m²/g, see Table S5) and to insoluble hypercrosslinked di-block PEO-*b*-PS particles (50-1123 m²/g). Pore sizes were calculated using NLDFT pore size analysis (Figure 3b) and confirmed the presence of micropores within the sample with a pore size distribution centred around 1.8 nm in the micropore region. Further meso- and macropores are also present within the samples which might be expected for particles with an aggregate morphology. The cumulative surface area vs pore width (Figure 3c) confirms that the surface area attributed to micropores increases with increasing particle size. Between 30 – 42% of the total surface area is attributed to micropores.

Table 2. Surface area and pore volumes of PPD samples.

Sample	Surface area (m²/g)[a]	Total pore volume (cm³/g)[b]	Micropore volume (cm³/g)[c]	Micropore/ total pore volume
PEG$_{113}$DVB$_{150}$FN$_{113}$	244	0.48	0.09	0.19
PEG$_{113}$DVB$_{300}$FN$_{225}$	270	0.45	0.10	0.20
PEG$_{113}$DVB$_{600}$FN$_{450}$	409	0.79	0.14	0.18
PEG$_{113}$DVB$_{1200}$FN$_{900}$	400	0.67	0.14	0.21

[a] calculated over the pressure range $0.01 – 0.15$ P/P$_0$, [b] calculated at 0.99 P/P$_0$, [c] calculated at 0.1 P/P$_0$

The particles were found to exhibit photoluminescence both in the solid state and in solution (λ_{max} = 320-330 nm, Figure S16), despite no extended conjugation within the particles. The λ_{max} of the particles is similar to that of the DVB monomer in solution. The luminescence is likely a result of the high density of aromatic rings within the core of the particles resulting in π-π stacking of the aromatic rings. The particles demonstrated bright blue fluorescence when excited by UV light which can easily be observed by eye in contrast to the DVB monomer solution.

The particle fluorescence was found to be selectively quenched by the addition of nitroaromatic compounds (Figure S15) such as picric acid – a known explosive and environmentally harmful compound. Upon addition of 38 ppm of picric acid the fluorescence of each sample was quenched by over 99% (Figure S17 & Table S6). This is superior to microporous polymers such as Py-Azine COF (69 %, 70 ppm of picric acid)[9] and Py-azo-COP (60 %, 0.96mM picric acid).[48] The limit of detection for PEG$_{113}$DVB$_{300}$FN$_{225}$ (Figure. S20), when exposed to picric acid, was found to be 169 ppb. This is comparable with other porous polymers possessing fluorescent sensing capabilities.[49, 50]

Quenching of the fluorescence of the DVB monomer by picric acid was also observed in solution (Figure. S21) and is the result of the interaction between the electron rich DVB monomer and electron deficient picric acid. In a similar way, the quenching mechanism observed in the porous particles is likely the result of the donor-acceptor electron-transfer interaction between the electron rich porous core and electron deficient quencher similar to that of other porous polymers.[49, 51-53] The ease with which the particles are dispersed combined with their ability to be collected after detection demonstrates the benefits of these materials over that of both soluble monomers and insoluble porous materials.

Conclusions

In conclusion soluble porous polymer particles were able to be synthesised *via* a versatile one-pot RAFT-mediated PISA synthesis using a PEG based macro-CTA with DVB and FN. It was possible to tune the size of the particles by increasing the ratio of core-forming monomers which resulted in an increase in internal porosity of the particles from 244 to 409 m²/g. Analysis of the samples by SAXS and TEM showed that the samples are present as mass fractals which are formed through aggregation of smaller particles. Aggregates ranged in size from 239 – 279 nm according to SAXS which was in close agreement to the DLS data (204 – 262 nm). Finally, these samples demonstrated fluorescence when exposed to UV light (Figures S15), which could be selectively quenched in the presence of nitroaromatic compounds, such as picric acid (38 ppm). This solution phase application highlights the potential new avenues for porous polymers. We believe that this is a versatile and facile synthetic route to dispersible porous polymers which offers the opportunity to change both the outer solubilising group and the inner porous core and has the potential to expand the range of applications available to porous materials.

Conflicts of interest

There are no conflicts to declare.

Acknowledgements

Notes and references

1. R. Dawson, A. I. Cooper and D. J. Adams, *Prog. Polym. Sci.*, 2012, **37**, 530-563.
2. N. Chaoui, M. Trunk, R. Dawson, J. Schmidt and A. Thomas, *Chem. Soc. Rev.*, 2017, **46**, 3302-3321.
3. M. E. Boot-Handford, J. C. Abanades, E. J. Anthony, M. J. Blunt, S. Brandani, N. Mac Dowell, J. R. Fernandez, M.-C. Ferrari, R. Gross, J. P. Hallett, R. S. Haszeldine, P. Heptonstall, A. Lyngfelt, Z. Makuch, E. Mangano, R. T. J. Porter, M. Pourkashanian, G. T. Rochelle, N. Shah, J. G. Yao and P. S. Fennell, *Energy Environ. Sci.*, 2014, **7**, 130-189.
4. W. Wang, M. Zhou and D. Yuan, *J. Mater. Chem. A*, 2017, **5**, 1334-1347.
5. R. Dawson, T. Ratvijitvech, M. Corker, A. Laybourn, Y. Z. Khimyak, A. I. Cooper and D. J. Adams, *Polym. Chem.*, 2012, **3**, 2034-2038.
6. R. Dawson, E. Stöckel, J. R. Holst, D. J. Adams and A. I. Cooper, *Energy Environ. Sci.*, 2011, **4**, 4239-4245.

7.   D. D'Alessandro, B. Smit and J. Long, *Angew. Chem. Int. Ed.*, 2010, **49**, 6058-6082.
8.   R. Dawson, A. I. Cooper and D. J. Adams, *Polym. Int.*, 2013, **62**, 345-352.
9.   S. Dalapati, S. Jin, J. Gao, Y. Xu, A. Nagai and D. Jiang, *J. Am. Chem. Soc.*, 2013, **135**, 17310-17313.
10.   K. Jiang, T. Fei and T. Zhang, *Sens. Actuators B*, 2014, **199**, 1-6.
11.   K. Jiang, D. Kuang, T. Fei and T. Zhang, *Sens. Actuators B*, 2014, **203**, 752-758.
12.   N. A. Rakow, M. S. Wendland, J. E. Trend, R. J. Poirier, D. M. Paolucci, S. P. Maki, C. S. Lyons and M. J. Swierczek, *Langmuir*, 2010, **26**, 3767-3770.
13.   M. P. Tsyurupa, Z. K. Blinnikova, Y. A. Borisov, M. M. Ilyin, T. P. Klimova, K. V. Mitsen and V. A. Davankov, *J. Sep. Sci.*, 2014, **37**, 803-810.
14.   D. Bratkowska, A. Davies, N. Fontanals, P. A. G. Cormack, F. Borrull, D. C. Sherrington and R. M. Marcé, *J. Sep. Sci.*, 2012, **35**, 2621-2628.
15.   M. Rose, *ChemCatChem*, 2014, **6**, 1166-1182.
16.   P. Kaur, J. T. Hupp and S. T. Nguyen, *ACS Catal.*, 2011, **1**, 819-835.
17.   L. Tan and B. Tan, *Chem. Soc. Rev.*, 2017, **46**, 3322-3356.
18.   J. Huang and S. R. Turner, *Polym. Rev.*, 2018, **58**, 1-41.
19.   N. B. McKeown, P. M. Budd, K. J. Msayib, B. S. Ghanem, H. J. Kingston, C. E. Tattershall, S. Makhseed, K. J. Reynolds and D. Fritsch, *Chem. Eur. J.*, 2005, **11**, 2610-2620.
20.   P. M. Budd, B. S. Ghanem, S. Makhseed, N. B. McKeown, K. J. Msayib and C. E. Tattershall, *Chem. Commun.*, 2004, DOI: 10.1039/b311764b, 230-231.
21.   Y. Xu, S. Jin, H. Xu, A. Nagai and D. Jiang, *Chem. Soc. Rev.*, 2013, **42**, 8012-8031.
22.   J. X. Jiang, F. Su, A. Trewin, C. D. Wood, N. L. Campbell, H. Niu, C. Dickinson, A. Y. Ganin, M. J. Rosseinsky, Y. Z. Khimyak and A. I. Cooper, *Angew. Chem. Int. Ed.*, 2007, **46**, 8574-8578.
23.   A. I. Cooper, *Adv. Mater.*, 2009, **21**, 1291-1295.
24.   G. Zhang, Z.-A. Lan and X. Wang, *Angew. Chem. Int. Ed.*, 2016, **55**, 15712-15727.
25.   Z. Yun-Bing and Z. Zhuang-Ping, *Chem. Asian J.*, 2018, **13**, 9-19.
26.   P. J. Waller, F. Gándara and O. M. Yaghi, *Acc. Chem. Res.*, 2015, DOI: 10.1021/acs.accounts.5b00369.
27.   J. L. Segura, M. J. Mancheno and F. Zamora, *Chem. Soc. Rev.*, 2016, **45**, 5635-5671.
28.   C.-Y. Lin, D. Zhang, Z. Zhao and Z. Xia, *Adv. Mater.*, 2018, **30**, 1703646-n/a.
29.   B. Florian and G. Bappaditya, *Angew. Chem. Int. Ed.*, 2018, **57**, 4850-4878.
30.   X. Feng, X. Ding and D. Jiang, *Chem. Soc. Rev.*, 2012, **41**, 6010-6022.
31.   S.-Y. Ding and W. Wang, *Chem. Soc. Rev.*, 2013, **42**, 548-568.
32.   P. Puthiaraj, Y.-R. Lee, S. Zhang and W.-S. Ahn, *J. Mater. Chem. A*, 2016, **4**, 16288-16311.
33.   P. Kuhn, M. Antonietti and A. Thomas, *Angew. Chem. Int. Ed.*, 2008, **47**, 3450-3453.
34.   A. Deshmukh, S. Bandyopadhyay, A. James and A. Patra, *J. Mater. Chem. C*, 2016, **4**, 4427-4433.
35.   G. Cheng, T. Hasell, A. Trewin, D. J. Adams and A. I. Cooper, *Angew. Chem. Int. Ed.*, 2012, **51**, 12727-12731.

36.   Y. Yang, B. Tan and C. D. Wood, *J. Mater. Chem. A*, 2016, **4**, 15072-15080.
37.   W. Mai, B. Sun, L. Chen, F. Xu, H. Liu, Y. Liang, R. Fu, D. Wu and K. Matyjaszewski, *J. Am. Chem. Soc.*, 2015, **137**, 13256-13259.
38.   F. Xie, W. Hu, L. Ding, K. Tian, Z. Wu and L. Li, *Polym. Chem.*, 2017, **8**, 6106-6111.
39.   H. Xu, J. Wu, B. Zheng, W. Mai, F. Xu, L. Chen, H. Liu, R. Fu, D. Wu and K. Matyjaszewski, *Chem. Commun.*, 2017, **53**, 5294-5297.
40.   T. N. Gao, T. Wang, W. Wu, Y. Liu, Q. Huo, Z. A. Qiao and S. Dai, *Adv. Mater.*, 2019, **31**, 1806254.
41.   C. Gao, H. Zhou, Y. Qu, W. Wang, H. Khan and W. Zhang, *Macromolecules*, 2016, **49**, 3789-3798.
42.   D. J. Kinning and E. L. Thomas, *Macromolecules*, 1984, **17**, 1712-1718.
43.   W.-D. He, X.-L. Sun, W.-M. Wan and C.-Y. Pan, *Macromolecules*, 2011, **44**, 3358-3365.
44.   N. P. Truong, M. V. Dussert, M. R. Whittaker, J. F. Quinn and T. P. Davis, *Polymer Chemistry*, 2015, **6**, 3865-3874.
45.   C. Wilson, M. J. Main, N. J. Cooper, M. E. Briggs, A. I. Cooper and D. J. Adams, *Polymer Chemistry*, 2017, **8**, 1914-1922.
46.   K. Venkata Rao, R. Haldar, T. K. Maji and S. J. George, *Physical Chemistry Chemical Physics*, 2016, **18**, 156-163.
47.   K. V. Rao, S. Mohapatra, T. K. Maji and S. J. George, *Chemistry – A European Journal*, 2012, **18**, 4505-4509.
48.   S. K. Gupta, D. Kaleeswaran, S. Nandi, R. Vaidhyanathan and R. Murugavel, *ACS Omega*, 2017, **2**, 3572-3582.
49.   H. Ma, B. Li, L. Zhang, D. Han and G. Zhu, *J. Mater. Chem. A*, 2015, **3**, 19346-19352.
50.   R. Sun, X. Huo, H. Lu, S. Feng, D. Wang and H. Liu, *Sens. Actuators B*, 2018, **265**, 476-487.
51.   Z. Xiang and D. Cao, *Macromol. Rapid Commun.*, 2012, **33**, 1184-1190.
52.   S. Wang, Y. Liu, Y. Yu, J. Du, Y. Cui, X. Song and Z. Liang, *New J. Chem.*, 2018, **42**, 9482-9487.
53.   D. Chen, C. Liu, J. Tang, L. Luo and G. Yu, *Polym. Chem.*, 2019, **10**, 1168-1181.

Polymer Chemistry Accepted Manuscript